

View Article Online **PAPER**



Cite this: Nanoscale, 2019, 11, 6174

Fly-through synthesis of nanoparticles on textile and paper substrates†

Miaolun Jiao, † Yonggang Yao, † Glenn Pastel, † Tangyuan Li, Zhigiang Liang, Hua Xie, Weiging Kong, Boyang Liu, Jianwei Song and Liangbing Hu **D**

The fast and efficient synthesis of nanoparticles on flexible and lightweight substrates is increasingly critical for various medical and wearable applications. However, conventional high temperature (high-T) processes for nanoparticle synthesis are intrinsically incompatible with temperature-sensitive substrates, including textiles and paper (i.e. low-T substrates). In this work, we report a non-contact, 'fly-through' method to synthesize nanoparticles on low-T substrates by rapid radiative heating under short timescales. As a demonstration, textile substrates loaded with platinum (Pt) salt precursor are rapidly heated and quenched as they move across a 2000 K heating source at a continuous production speed of 0.5 cm s⁻¹. The rapid radiative heating method induces the thermal decomposition of various precursor salts and nanoparticle formation, while the short duration ensures negligible change to the respective low-T substrate along with greatly improved production efficiency. The reported method can be generally applied to the synthesis of metal nanoparticles (e.g. gold and ruthenium) on various low-T substrates (e.g. paper). The non-contact and continuous 'fly-through' synthesis offers a robust and efficient way to synthesize supported nanoparticles on flexible and lightweight substrates. It is also promising for ultrafast and rollto-roll manufacturing to enable viable applications.

Received 16th December 2018. Accepted 10th March 2019 DOI: 10.1039/c8nr10137j

rsc.li/nanoscale

Introduction

Supported nanoparticles are widely used in the fields of plasmonics, catalysis, energy storage, antibiosis, and energy conversion. 1-5 The fast and efficient synthesis of supported nanoparticles is in urgent demand to promote their viable applications. 6-10 Conventionally, high-temperature (high-T) methods, such as annealing, thermal reduction and calcination, offer favorable thermodynamic environments for efficient and controlled nanoparticle synthesis. 11-13 In addition, high-T methods with a shorter duration time, such as microwave radiation as well as flame synthesis methods, can produce supported nanoparticles within several minutes or even seconds. 14-22 These simple and physical deposition methods based on high temperature processes are easily scalable and sustainable with minimal chemical pollutants and solution waste, and are favorable for efficient synthesis of supported

However, these methods heat the entire sample to high temperatures and have seldom been demonstrated for sub-

Department of Materials Science and Engineering, University of Maryland, College Park, Maryland, 20742, USA. E-mail: binghu@umd.edu

strates with low thermal stability, such as textiles and paper (i.e. low-T substrates), as the structure of these substrates is easily compromised in the heating process. Yet, nanoparticles dispersed on flexible and lightweight low-T substrates are increasingly critical for various medical and wearable applications (e.g. antibacterial surfaces, disease detection, and biosensing), where large-scale and low-cost products are used.23-26 These medical and wearable applications require a facile, scalable particle synthesis method that is also compatible with low-T substrates. 27-30 Therefore, it is crucial to overcome the dichotomy between 'efficient high-T synthesis' and 'sensitive low-T substrates' to enable the rapid synthesis of nanoparticles on flexible substrates in a scalable and sustainable manner.

For the first time, we report a one-step, 'fly-through' method to synthesize well-dispersed nanoparticles on low-T substrates (i.e. textiles and paper) via high-temperature, rapid radiative heating. In a typical process, the metal precursor loaded textile is pulled across the top (0.5 cm away) of the high-T heating source (2000 K) at a constant rate of 0.5 cm s⁻¹, after which the metal nanoparticles are uniformly dispersed on the textile. The high-temperature source enables the decomposition of the precursor salts and nanoparticle nucleation on the surface of the textile. In addition, the continuous 'fly-through' synthesis with limited short heating duration only leads to uniform nanoparticle formation while avoiding

[†]Electronic supplementary information (ESI) available. See DOI: 10.1039/ c8nr10137j

[‡]These authors contributed equally to this work.

deterioration of the textile substrate. The non-destructive 'flythrough' method is generally applicable for the synthesis of other metal nanoparticles (e.g. Au and Ru) on various low-T substrates (e.g. paper). The non-contact and continuous particle synthesis is deemed compatible with roll-to-roll processes for scalable and ultrafast nanomanufacturing.

Results and discussion

The one-step, rapid radiative heating process is depicted in Fig. 1a. The H₂PtCl₆ precursor loaded textile is pulled across the high-T heating source quickly to induce nanoparticle formation by high-temperature radiation and subsequent quenching. The high intensity of the thermal radiation leads to the decomposition of the H₂PtCl₆ precursor and transformation into Pt nanoparticles on the surface of the textile in several seconds. Owing to the short duration of the high temperature treatment process, the structure of the textile maintains largely intact and avoids high-temperature induced significant degradation. Therefore, the radiative heating method is uniquely suited to synthesizing metal nanoparticles on low-T textiles by limiting the high temperature duration and is similarly conducive to promote the production efficiency compared to conventional longtime heating nanoparticle synthesis methods.

To load the salt precursor, the textiles were soaked in H₂PtCl₆ precursor solution (0.05 mol L⁻¹ H₂PtCl₆ in ethanol) for 20 min before drying in air for 1 h. The SEM images in Fig. S1a and b† show the crosswise aligned fibers loaded with H₂PtCl₆ precursor, and the enlarged SEM image in Fig. 1b reveals that the 200-400 nm salt crystals are sparsely dispersed on the surface of the textile fibers. In contrast, after the radiative heating process, numerous Pt nanoparticles are uniformly distributed on the textile with particle sizes between 60–140 nm (Fig. 1c). Simultaneously, the surfaces of the fibers are largely unperturbed after the rapid radiative heating method and retain their configuration. The H₂PtCl₆ precursor decomposition is further verified by the energy dispersive spectrum (EDS) displayed in Fig. 1d. The chloride (Cl) peak decreases substantially in samples after the radiative heating treatment, indicating that most of the Cl element (in Pt salt) is gone after thermal decomposition and leaves metallic Pt nanoparticles. The synthesized Pt nanoparticles were also characterized by XRD (Fig. S2†) and TEM (Fig. S3†), confirming the particle size and crystalline metallic structure.31 Therefore, by rapid radiative heating, precursor salt can decompose under a short duration and nucleate into metal nanoparticles without significant altercation to the textile fibers.

The tunable parameters of the radiative heating method for supported nanoparticles production are introduced in Fig. 2,

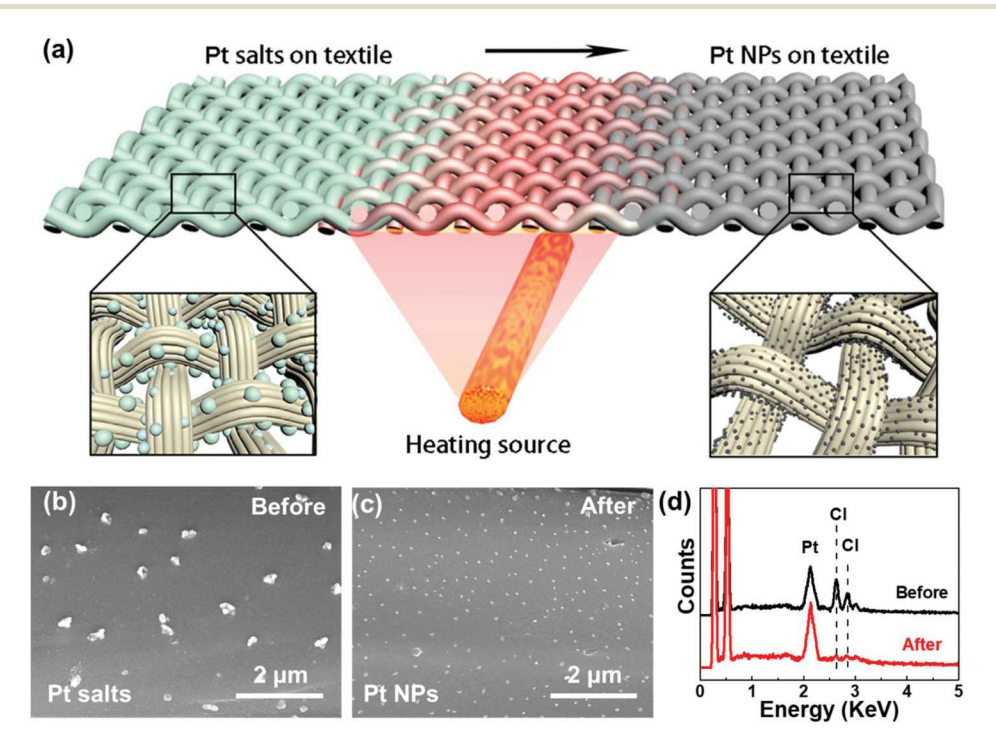


Fig. 1 (a) Schematic of the 'fly-through' synthesis of Pt nanoparticles on textiles by the rapid radiative heating method. The H₂PtCl₆ precursor loaded textile is pulled across the high-T heating source at a continuous rate of 0.5 cm s⁻¹. The radiation from the high-temperature source induces decomposition of salt precursor and nucleates Pt nanoparticles on the surface of the textile while keeping the low-T substrate intact due to the short heating duration. The morphology of the textile with H₂PtCl₆ precursor (b) before and (c) after radiative heating. (d) The EDS spectrum of the textile with H₂PtCl₆ precursor before and after radiative heating.

Paper

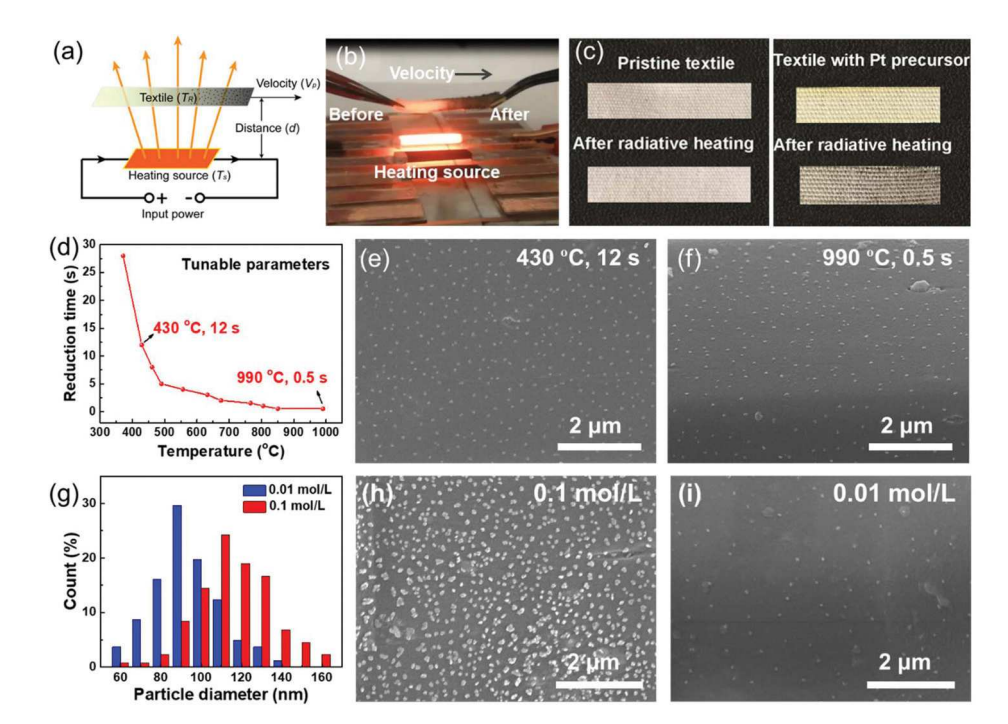


Fig. 2 Kinetic control in the rapid radiative heating process. (a) A side-view schematic detailing the pertinent parameters of the radiative heating method. (b) The corresponding side-view image of the radiative heating process in which a precursor-loaded textile is pulled across the emissive heating source. (c) Photographs of a pristine and precursor-loaded textile before and after undergoing the radiative heating method, respectively. (d) The relationship between the temperature and the reduction time for the Pt nanoparticle formation. The morphology of the Pt nanoparticles on the textile through (e) radiative heating at 430 °C for 12 s and (f) radiative heating at 990 °C for 0.5 s. (g) The size distribution of the Pt nanoparticles on textiles soaked in 0.1 mol L^{-1} and 0.01 mol L^{-1} precursor solutions, and their corresponding SEM images in (h) and (i), respectively.

showing the 'fly-through' process as a flexible yet robust synthesis method. Fig. 2a illustrates the setup of the rapid radiative heating method and the processing parameters including the radiative source temperatures (T_s) , the working distance between the heating source and low-T substrate (d), and the moving/production speed (V_p) . In our experiment, carbon nanofiber (CNF) films are used as radiative heating sources, which can be heated up to 3000 K by electrical Joule heating and controlled easily by adjusting the electrical input.³² Fig. 2b shows the H₂PtCl₆ precursor loaded textile being pulled across the radiative heating zone ($T_{\rm s} \sim 2000$ K, Fig. S4a†), 0.5 cm from the emissive source, at a velocity of $0.5~{\rm cm~s^{-1}}$. The surface of the textile noticeably changes black after moving through high temperature heating source while the rest of textile is still a pristine white color. Control tests on pristine textiles without salt precursor show no change in color or morphology after radiative heating (Fig. 2c), thereby indicating that the rapid heating does not induce significant decomposition or carbonization of the textile substrate. To reiterate, the color of the precursorloaded textile changes from yellow (with H₂PtCl₆ precursor) to black tint, which can be attributed to the precursor decomposition and nanoparticle formation (Fig. 2c, right). The black tint is the result of light absorption by the asformed Pt nanoparticles owing to the plasmonic effect. 33,34 Consequently, the color change in the textile is an important indicator of nanoparticle formation on textile during the radiative heating process.

The rapid radiative heating process can be easily tuned for the synthesis of supported nanoparticles. The temperature for the radiative heating (T_R) is important for the decomposition of the precursor salts and it can be adjusted by the electrical input (Fig. S4b†) and working distance (Fig. S4c†) between 350 and 1000 °C. According to each specific $T_{\rm R}$, there is a corresponding particle formation time as identified according to the color change on the textile, and confirmed through ex situ measurements. Higher radiative temperatures require shorter radiative heating durations in the production process, as shown in Fig. 2d. Although the synthesis temperature varies significantly, surprisingly, similar Pt nanoparticle distributions on the textile are shown in Fig. 2e and f, which are radiative heated at 430 °C for 12 s and 990 °C for 0.5 s, respectively. This indicates that the rapid radiative heating process renders similar size distributions as long as the salt precursor is completely decomposed. Therefore, the processing parameters in the radiative heating process can be easily adjusted for similar nanoparticles synthesis on textile substrates, thereby demonstrating its flexible and robust production capability.

In addition, by tuning the initial salt concentration on the textile material, the particle size and distribution can be adjusted. As demonstrated in Fig. 2g, soaking the textile in

H₂PtCl₆ precursor solution with 0.1 mol L⁻¹ and 0.01 mol L⁻¹ concentrations result in different particle size distributions centered around 110 nm and 90 nm nanoparticles, respectively, according to the SEM images in Fig. 2h and i. The high concentration specimen (0.1 mol L⁻¹) shows a dense scattering of Pt nanoparticles on the surface of the textile fibers after radiative heating. In contrast, the low concentration specimen (0.01 mol L⁻¹) demonstrates a sparse scattering of nanoparticles that are ~20 nm smaller on average (Fig. 2i). Therefore, the particle diameter and loading density of the supported nanoparticles on the textile are tunable through adjustments to the initial salt loading.

The morphology, durability, and uniformity of the textile before and after radiative heating were studied by optical microscopy, FT-IR, tensile tests, and XRD, as shown in Fig. 3. Optical microscope images (Fig. 3a and b) further illustrate that the textile is not damaged or carbonized after radiative heating. The brown color of the substrate after radiative heating, again, indicates the formation of Pt nanoparticles that absorb visible light, rather than potential damage to the textile (refer to Fig. S5† for the optical microscopic images of a

pristine substrate before and after radiative heating). The functional groups of these samples were also tested by FT-IR spectroscopy (Fig. 3c). The O-H $(3328.58 \text{ cm}^{-1})$, C-H (2913.96 cm⁻¹), C=O (1712.5 cm⁻¹), and C-O (1241.95 cm⁻¹, 1095.39 cm⁻¹, 1016.32 cm⁻¹) remain the same after the radiative heating process, proving negligible carbonization during the radiative heating process.35 In addition, the mechanical strength of textile samples before and after radiative heating was measured with a Tinius Olsen H5KT tester. As shown in Fig. 3d, the strength of the Pt nanoparticle loaded textile (45.9 MPa) is similar to that of the pristine textile (50.7 MPa), indicating the physical structure of the textile is maintained after the ultrafast radiative heating process. We also verified the structure of the textile before and after radiative heating by XRD (Fig. S2†). In the XRD spectra, the peaks at 13.64°, 16.76°, and 22.67° belong to cotton, and the 26.01° peak is attributed to polyester, 36 which persist after the radiative heating process. All the above results from microscopy images, FT-IR, tensile tests, and XRD illustrate that the physical and chemical structure of the textile is retained after the ultrafast radiative heating process.

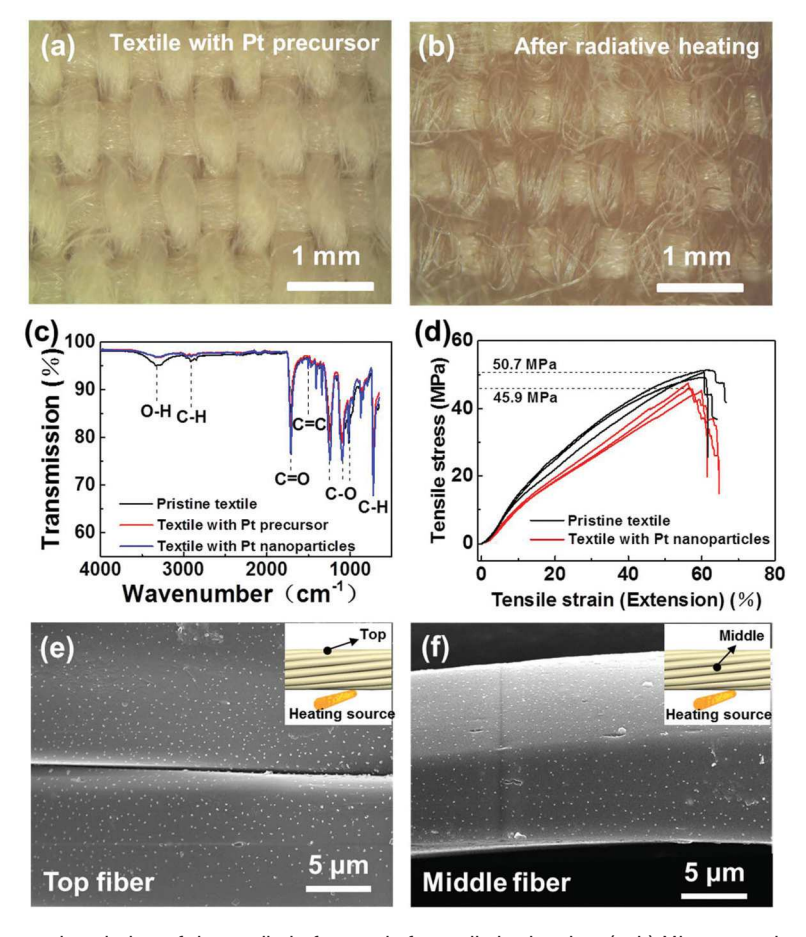


Fig. 3 Morphological and structural evolution of the textile before and after radiative heating. (a, b) Microscopy images of the textile with precursors before and after radiative heating, respectively, the black color is due to the synthesis of nanoparticles on the textile after radiative heating; (c) FT-IR of the pristine textile, the textile with Pt precursor, and the textile after radiative heating; (d) the mechanical strength of the textile with Pt precursors before and after radiative heating; (e, f) the uniformity of the Pt nanoparticles along the top and middle orientations of the textile (refer to the radiative source).

Paper Nanoscale

The uniformity of the Pt nanoparticles throughout the textile substrate is verified to understand the directionality of the radiative heating process. As the radiative heating process is applied to only one side of the substrate, the surface area indirectly heated by the radiative source is investigated by SEM. On the fiber oriented away from the radiative heating source, the Pt nanoparticles are uniformly dispersed with morphologies consistent with nanoparticles directly facing the radiative heating source (Fig. 3e). Nanoparticles formed along the middle of the fiber are also similar in size and dispersion from the rest of the textile (Fig. 3f, also Fig. S6†). Therefore, at an active working distance of 0.5 cm, there is little to differentiate the nanoparticles given their location on the textile. These observations indicate that the synthesis is relatively invariable with the orientation of the radiative heating source, so long as the intensity of the radiative source is high enough to prompt thermal decomposition of the precursor materials on the surface of the textiles.

Given the temperatures (990 °C) achieved during the radiative heating method, this approach can be adapted to form various metal nanoparticles on low-T substrates by thermal decomposition of other salt precursors. As shown in Fig. 4b and c, Au and Ru nanoparticles can be uniformly dispersed on textile substrates by the same radiative heating process,

thereby demonstrating the transferability of this method to other material systems. As with the Pt nanoparticle based textiles, the substrates blanketed with Au and Ru nanoparticles show negligible degradation after radiative heating. However, the precursor salts do show varying decomposition temperatures and affinities to the low-T substrates which is manifested by varying particle sizes and distributions.³⁷

The structural integrity of fragile low-T substrates after the rapid 'fly-through' synthesis is one of the most surprising and exciting aspects of this approach and also can be easily extend to other substrates. Feather-weight paper (a typical low-T substrates) used in these experiments are loosely knit to better store the precursor salts without any additives on the surface of the substrate (Fig. 4d). Using the same radiative heating process, Pt and Au nanoparticles can be uniformly dispersed on the feather-weight paper substrate with a size distribution between 50–80 nm and 100–240 nm, respectively (Fig. 4e and f). The differential particle diameters of the Pt and Au nanoparticles are decided by the decomposed temperature and the affinity of the metals. Therefore, this rapid radiative heating method is an appealing method to synthesize uniform nanoparticles on the porous and flexible low-T substrates.

The ultrafast, roll-to-roll manufacturing of the rapid radiative heating process for low-T substrates is envisioned using

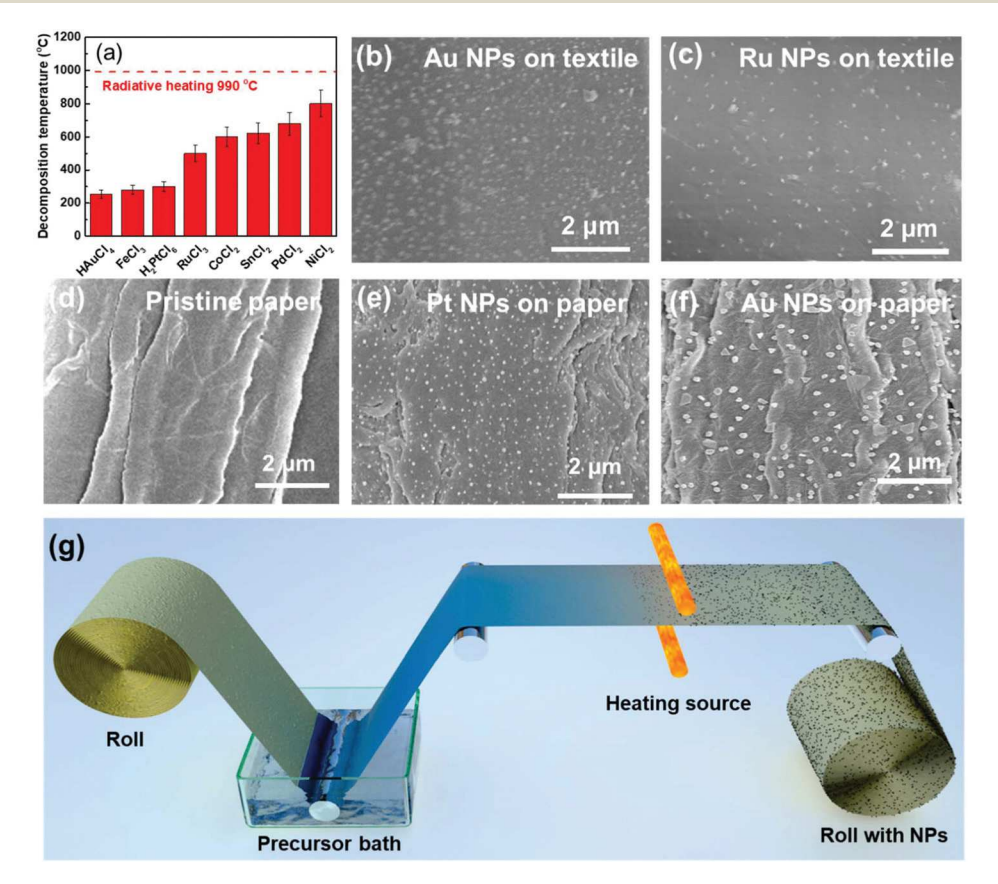


Fig. 4 The universality of the radiative heating on flexible substrates. (a) The decomposition temperature for different precursor salts, which usually can be decomposed under the radiative heating temperature. The microstructure of pristine paper (d) as well as paper loaded with Pt (e) and Au (f) nanoparticles. (g) Schematic of roll-to-toll manufacturing of nanoparticles by the radiative heating method on low-T substrates.

Nanoscale Paper

the schematic in Fig. 4g. In the roll-to-roll process, a low-T substrate is immersed in a precursor bath and then passes by the radiative heating source for rapid synthesis of metal nanoparticles. In particular, this approach is made possible by the flexibility of the low-T substrates and the rapid, non-contacting radiative heating method. Therefore, the synthesis of nanoparticles on the low-T substrates through the rapid and noncontact radiative heating method is compatible with existing industrial protocols, which holds great promise towards ultrafast, roll-to-roll nanomanufacturing of various supported nanoparticles.

Conclusions

For the first time, we report a "fly-through" method to synthesize uniform nanoparticles on temperature-sensitive substrates (e.g. textiles and paper) by rapid high-temperature radiative heating. The high temperatures achieved from the heating source lead to the thermal decomposition of the precursor salts and formation of metal nanoparticles on the surface of the substrates. The ultrafast radiative heating process ensures the low-T substrates (textiles and papers) remain intact after nanoparticle formation. The non-contact "fly-through" method offers a robust and efficient way to synthesize supported nanoparticles on cheap, flexible, and temperature-sensitive substrates. This continuous particle production method is also deemed compatible with conventional roll-to-roll processes for scalable nanomanufacturing.

Experimental section

Preparation of the metal precursor loaded textile and paper

Prepare 0.05 mol L^{-1} H_2PtCl_6 solution, 0.05 mol L^{-1} H_2AuCl_6 solution, and 0.05 mol L^{-1} $RuCl_3$ solution (ethanol was used as the solvent) as the precursor of Pt, Au, and Ru nanoparticles, respectively. The textile in the experiments, composed of cotton and polyester, is cut into 5 cm \times 1 cm strips. The textile strips are immersed into the precursor solution and soaked for 20 min, then dried for 1 hour at room temperature. The as-prepared precursor loaded textile was used without further modification for the rapid radiative heating experiments. The feather-weight papers were tested as other low-T substrates, using the same method as the textile specimens.

Preparation of the radiative heating source

The radiative heating source consists of PAN-based carbon nanofibers (CNF), which are prepared by electrospinning. The 8 wt% polyacrylonitrile (PAN) in dimethylformamide (DMF) solvent is electrospun at a voltage of 10 kV, a spinning distance of 15 cm, an extrusion rate of 1 mL h $^{-1}$, and a collector rotation speed of 80 rpm. Then, the electrospun fibers are stabilized at 240 °C for 6 h in air and carbonized at 900 °C for 2 hours in argon. The resultant carbon nanofiber mat is cut

into 2 cm \times 0.5 cm strips and attached to copper electrodes with the silver paste. The carbon nanofibers are capable of bearing a high Joule heating load with a local temperature of 3000 K. A Keithley 2425 Source Meter serves as the external electrical power source.

Rapid radiative heating process

The rapid radiative heating process was conducted in an argon filled glovebox. When the radiative heating source reaches 2000 K, the precursor loaded textile is continuously pulled across the high temperature heating zone at a distance of 0.5 cm with a speed of 0.5 cm s⁻¹. The power of the external power source, the distance between the heating source and textile samples, and the velocity of the textile samples across the heating zone can be tuned to vary the working temperature and the reaction time, through which the metal nanoparticles loaded textile can be fabricated evenly. The Au and Ru NPs loaded textiles are prepared by the same method as well as the porous Pt and Au NPs loaded paper samples.

Characterization

The morphology of the prepared samples was observed with a Tescan XEIA FEG SEM at 5 kV. Mechanical tensile properties were measured on a Tinius Olsen H5KT tester, and FT-IR spectrum was carried out on a Thermo Nicolet NEXUS 670 FT-IR. The X-ray diffusion (XRD) was tested by a D8 Advanced system (Bruker AXS, WI, USA) using a Cu K α radiation source at 40 kV and 40 mA. A thermoelectric couple was used to test the temperature at a certain distance from the heating source, which is the operating heating temperature of the rapid radiative heating method. The temperature of the heating source was tested by collecting the emitted light (Ocean Optics spectrometer) and fitting the emitted light spectrum to a gray body radiation curve.

Conflicts of interest

There are no conflicts to declare.

Acknowledgements

This work is supported by the NSF Scalable Nanomanufacturing Project No. 1635221. We acknowledge the support of the Maryland Nanocenter and AIMLab. We acknowledge to Yangkai Chen for schematic drawing. M. Jiao acknowledges the financial support by the China Scholarship Council (CSC).

References

1 S. H. Joo, J. Y. Park, C. K. Tsung, Y. Yamada, P. Yang and G. A. Somorjai, Thermally stable Pt/mesoporous silica coreshell nanocatalysts for high-temperature reactions, *Nat. Mater.*, 2009, 8(2), 126–131.

Paper

- 2 L. Liu and A. Corma, Metal Catalysts for Heterogeneous Catalysis: From Single Atoms to Nanoclusters and Nanoparticles, Chem. Rev., 2018, 118(10), 4981-5079.
- 3 A. K. Yetisen, H. Qu, A. Manbachi, H. Butt, M. R. Dokmeci, J. P. Hinestroza, M. Skorobogatiy, A. Khademhosseini and S. H. Yun, Nanotechnology in Textiles, ACS Nano, 2016, **10**(3), 3042-3068.
- 4 S. Xu, Y. Chen, Y. Li, A. Lu, Y. Yao, J. Dai, Y. Wang, B. Liu, S. D. Lacey, G. R. Pastel, Y. Kuang, V. A. Danner, F. Jiang, K. K. Fu and L. Hu, Universal, In Situ Transformation of Bulky Compounds into Nanoscale Catalysts by High-Temperature Pulse, Nano Lett., 2017, 17(9), 5817-5822.
- 5 H. A. Atwater and A. Polman, Plasmonics for improved photovoltaic devices, Nat. Mater., 2010, 9(3), 205-213.
- 6 M. Mizuno, Y. Sasaki, A. C. Yu and M. Inoue, Prevention of nanoparticle coalescence under high-temperature annealing, Langmuir, 2004, 20(26), 11305-11307.
- 7 C. Ritchie, A. S. R. Chesman, M. Styles, J. J. Jasieniak and Synthesis Mulvaney, Aqueous of High-Quality Cu2ZnSnS4 Nanocrystals and Their Thermal Annealing Characteristics, Langmuir, 2018, 34(4), 1655-1665.
- 8 L. Xiong, M. Qin, C. Chen, J. Wen, G. Yang, Y. Guo, J. Ma, Q. Zhang, P. Qin, S. Li and G. Fang, Fully High-Temperature-Processed SnO2 as Blocking Layer and Scaffold for Efficient, Stable, and Hysteresis-Free Mesoporous Perovskite Solar Cells, Adv. Funct. Mater., 2018, 28(10), 1706276.
- 9 D. Childers, A. Saha, N. Schweitzer, R. M. Rioux, J. T. Miller and R. J. Meyer, Correlating Heat of Adsorption of CO to Reaction Selectivity: Geometric Effects vs Electronic Effects in Neopentane Isomerization over Pt and Pd Catalysts, ACS Catal., 2013, 3(11), 2487-2496.
- 10 Y. Yao, F. Jiang, C. Yang, K. K. Fu, J. Hayden, C. F. Lin, H. Xie, M. Jiao, C. Yang, Y. Wang, S. He, F. Xu, E. Hitz, T. Gao, J. Dai, W. Luo, G. Rubloff, C. Wang and L. Hu, Epitaxial Welding of Carbon Nanotube Networks for Aqueous Battery Current Collectors, ACS Nano, 2018, 12(6), 5266-5273.
- 11 C.-L. Ye, C.-L. Guo and J.-L. Zhang, Highly active and stable CeO2-SiO2 supported Cu catalysts for the hydrogenation of methyl acetate to ethanol, Fuel Process. Technol., 2016, 143, 219-224.
- 12 M. Zhang, Q. Dai, H. Zheng, M. Chen and L. Dai, Novel MOF-Derived Co@N-C Bifunctional Catalysts for Highly Efficient Zn-Air Batteries and Water Splitting, Adv. Mater., 2018, 30(10), 1705431.
- 13 A. Salem, E. Saion, N. M. Al-Hada, H. M. Kamari, A. H. Shaari and S. Radiman, Simple synthesis of ZnSe nanoparticles by thermal treatment and their characterization, Results Phys., 2017, 7, 1175-1180.
- 14 H. Fei, J. Dong, C. Wan, Z. Zhao, X. Xu, Z. Lin, Y. Wang, H. Liu, K. Zang, J. Luo, S. Zhao, W. Hu, W. Yan, I. Shakir, Y. Huang and X. Duan, Microwave-Assisted Rapid Synthesis of Graphene-Supported Single Atomic Metals, Adv. Mater., 2018, 1802146.
- 15 D. Zhang, C. Chen, X. Wang, G. Guo and Y. Sun, Synthesis of PtAu Alloy Nanocrystals in Micelle Nanoreactors Enabled

- by Flash Heating and Cooling, Part. Part. Syst. Charact., 2018, 1700413.
- 16 V. Chikan and E. J. McLaurin, Rapid Nanoparticle Synthesis by Magnetic and Microwave Nanomaterials, 2016, 6(5), 85.
- 17 X. J. Shi, M. Fields, J. Park, J. M. McEnaney, H. P. Yan, Y. R. Zhang, C. Tsai, T. F. Jaramillo, R. Sinclair, J. K. Norskov and X. L. Zheng, Rapid flame doping of Co to WS2 for efficient hydrogen evolution, Energy Environ. Sci., 2018, 11(8), 2270-2277.
- 18 S. Li, Y. Ren, P. Biswas and S. D. Tse, Flame aerosol synthesis of nanostructured materials and functional devices: Processing, modeling, and diagnostics, Prog. Energy Combust. Sci., 2016, 55, 1-59.
- 19 F. Niu, S. Li, Y. Zong and Q. Yao, Catalytic Behavior of Flame-Made Pd/TiO2 Nanoparticles in Methane Oxidation at Low Temperatures, J. Phys. Chem. C, 2014, 118(33), 19165-19171.
- 20 S. Hannemann, J.-D. Grunwaldt, P. D. Günther, F. Krumeich, S. E. Pratsinis and A. Baiker, Combination of flame synthesis and high-throughput experimentation: The preparation of alumina-supported noble metal particles and their application in the partial oxidation of methane, Appl. Catal., A, 2007, 316(2), 226-239.
- 21 J. K. Kim, S. U. Chai, Y. Ji, B. Levy-Wendt, S. H. Kim, Y. Yi, T. F. Heinz, J. K. Nørskov, J. H. Park and X. Zheng, Resolving Hysteresis in Perovskite Solar Cells with Rapid Flame-Processed Cobalt-Doped TiO2, Adv. Energy Mater., 2018, 8(29), 1801717.
- 22 S. Q. Li, Y. H. Ren, P. Biswas and S. D. Tse, Flame aerosol synthesis of nanostructured materials and functional devices: Processing, modeling, and diagnostics, Prog. Energy Combust. Sci., 2016, 55, 1-59.
- 23 A. L. Hicks and T. L. Theis, A comparative life cycle assessment of commercially available household silver-enabled polyester textiles, Int. J. Life Cycle Assess., 2016, 22(2), 256-265.
- 24 J. Kumar, H. Erana, E. Lopez-Martinez, N. Claes, V. F. Martin, D. M. Solis, S. Bals, A. L. Cortajarena, J. Castilla and L. M. Liz-Marzan, Detection of amyloid fibrils in Parkinson's disease using plasmonic chirality, Proc. Natl. Acad. Sci. U. S. A., 2018, 115(13), 3225-3230.
- 25 L. Budama, B. A. Çakır, Ö. Topel and N. Hoda, A new strategy for producing antibacterial textile surfaces using silver nanoparticles, Chem. Eng. J., 2013, 228, 489-495.
- 26 S. Xu, Y. Yao, Y. Guo, X. Zeng, S. D. Lacey, H. Song, C. Chen, Y. Li, J. Dai, Y. Wang, Y. Chen, B. Liu, K. Fu, K. Amine, J. Lu and L. Hu, Textile Inspired Lithium-Oxygen Battery Cathode with Decoupled Oxygen and Electrolyte Pathways, Adv. Mater., 2018, 30(4), 1704907.
- 27 H. Ahmari, S. Z. Heris and M. H. Khayyat, The effect of titanium dioxide nanoparticles and UV irradiation on photocatalytic degradation of Imidaclopride, Environ. Technol., 2018, 39(4), 536-547.

28 C. Sun, Y. Li, Z. Li, Q. Su, Y. Wang and X. Liu, Durable and Washable Antibacterial Copper Nanoparticles Bridged by Surface Grafting Polymer Brushes on Cotton and Polymeric

Materials, J. Nanomater., 2018, 2018, 1-7.

- 29 E. Spielman-Sun, T. Zaikova, T. Dankovich, J. Yun, M. Ryan, J. E. Hutchison and G. V. Lowry, Effect of silver concentration and chemical transformations on release and anti-bacterial efficacy in silver-containing textiles, *NanoImpact*, 2018, 11, 51–57.
- 30 H. Lu, J. Chen and Q. Tian, Wearable high-performance supercapacitors based on Ni-coated cotton textile with low-crystalline Ni-Al layered double hydroxide nanoparticles, *J. Colloid Interface Sci.*, 2017, **513**, 342–348.
- 31 J. Shi, R. Nie, P. Chen and Z. Hou, Selective hydrogenation of cinnamaldehyde over reduced graphene oxide supported Pt catalyst, *Catal. Commun.*, 2013, 41, 101–105.
- 32 Y. Yao, Z. Huang, P. Xie, S. D. Lacey, R. J. Jacob, H. Xie, F. Chen, A. Nie, T. Pu, M. Rehwoldt, D. Yu, M. R. Zachariah, C. Wang, R. Shahbazian-Yassar, J. Li and

- L. Hu, Carbothermal shock synthesis of high-entropy-alloy nanoparticles, *Science*, 2018, **359**(6383), 1489–1494.
- 33 X. Zhang, Y. L. Chen, R. S. Liu and D. P. Tsai, Plasmonic photocatalysis, *Rep. Prog. Phys.*, 2013, 76(4), 046401.
- 34 P. Wang, B. Huang, Y. Dai and M. H. Whangbo, Plasmonic photocatalysts: harvesting visible light with noble metal nanoparticles, *Phys. Chem. Chem. Phys.*, 2012, **14**(28), 9813–9325.
- 35 E. Bozaci, B. Arik, A. Demir and E. Ozdogan, Potential Use of New Methods for Identification Of Hollow Polyester Fibres, *Tekst Konfeksiyon*, 2012, 22(4), 317–323.
- 36 F. Li, Y. Xing and X. Ding, Silica xerogel coating on the surface of natural and synthetic fabrics, *Surf. Coat. Technol.*, 2008, **202**(19), 4721–4727.
- 37 S. Lin, Y. Cheng, Y. Bobcombe, K. L. Jones, J. Liu and M. R. Wiesner, Deposition of silver nanoparticles in geochemically heterogeneous porous media: predicting affinity from surface composition analysis, *Environ. Sci. Technol.*, 2011, 45(12), 5209–5215.